J Mater Sci (2008) 43:6278–6284
DOI 10.1007/s10853-008-2904-7

Mesoporous niobium oxides with tailored pore structures

Li Yuan · Vadim V. Guliants

Received: 1 April 2008 / Accepted: 24 July 2008 / Published online: 13 August 2008

Abstract Novel thermally stable and 2D mesoporous niobia phases were prepared by the evaporation induced self-assembly (EISA) with high surface areas (up to 211 m^2/g). The pore size of these novel mesoporous niobium oxides was tuned in a wide range from 4.6 to 21 nm by increasing the aging temperature, aging time, and humidity of aging atmosphere. Mixtures of two nonionic surfactants, Pluronic P123 and Brij 35, were for the first time used to tune the pore structure of resultant mesoporous niobia phases which showed that the mesopore shape may be switched from cylindrical to ink-bottle. The niobia mesostructures obtained in this study were thermally stable up to 500 °C. These novel mesoporous niobium oxides with tunable pore sizes are highly promising as catalytic supports and a major component in the synthesis of porous Nb-containing mixed metal oxides, such as $MoVTeNbO_x$ catalysts for selective (amm)oxidation of propane.

Introduction

Niobium compounds are presently of great interest in heterogeneous catalysis where they are used as catalyst components, promoters, or supports. The vast majority of niobium-containing catalysts are based on niobium oxide species [1–6]. Niobium oxides remarkably enhance catalytic activity and prolong catalyst life as catalyst components or promoters. The addition of Nb_2O_5 to bismuth molybdate catalyst is well known to have a remarkable effect on the activity and selectivity for the oxidation and ammoxidation of ethylene [1]. According to Somorjai and his coworkers [2] the presence of Nb_2O_5 together with molybdenum and vanadium oxides was necessary for the high activity and selectivity of mixed metal oxide catalysts in the oxidative dehydrogenation of ethane which displayed the selectivity to ethylene as high as 93 mol%. In addition to being used as a catalytically active component or promoter, niobium oxides are highly useful as supports of metal and metal oxide catalysts. It was shown that Nb_2O_5 could be used to form 2D overlayers of vanadium, chromium, rhenium, molybdenum, and tungsten oxides [3]. These Nb_2O_5-supported metal oxides were successfully tested for the partial oxidation of methanol. It was observed that these Nb_2O_5-supported catalysts were able to convert methanol to formaldehyde with turnover frequencies comparable to or better than other supported metal oxide catalysts that used more traditional supports, such as Al_2O_3, SiO_2, and TiO_2 [4]. It appeared that Nb_2O_5-supported metal oxide catalysts are promising catalytic materials for selective oxidation reactions [5, 6].

High surface areas, accessible pore structures, decreased contribution of mass transfer effects, and high thermal stability are extremely desirable characteristics of heterogeneous catalysts [7–9]. A search for new high surface area niobium oxides primarily focused on the synthesis of ordered mesoporous niobium(V) oxides [10–16]. In their pioneering work, Ying and co-workers [10–12] introduced the ligand-assisted templating approach to synthesize first stable mesoporous Nb_2O_5. They pretreated amine surfactants with a Nb alkoxide in the absence of water to form metal-ligated surfactants which facilitated covalent interactions between the surfactant head group and niobium precursor. The addition of water initiated surfactant self-assembly, alkoxide hydrolysis, and metal oxide condensation. However, the template-free

L. Yuan · V. V. Guliants (✉)
Department of Chemical and Materials Engineering,
University of Cincinnati, Cincinnati, OH 45221-0012, USA
e-mail: yuanli@email.uc.edu

mesoporous niobium oxide obtained by this approach possessed small mesopores (<40 Å). Yang et al. [14] synthesized mesoporous Nb_2O_5 in nonaqueous media by using poly(alkylene oxide) block copolymers as structure-directing agents. It is believed [14] that crown-ether-type complexes formed between alkylene oxide segments and inorganic ions through weak coordination bonds. Mesoporous Nb_2O_5 obtained in their work possessed a mean pore size of 50 Å. The 3D hexagonal mesostructure of Nb_2O_5 was shown by Domen and coworkers [15, 16] when P-5 was used as a template employing electrostatic interactions between the neutral surfactant and ions. NaCl was also added to improve the mesostructure quality. The mesoporous Nb_2O_5 with pore size of 50 Å and wall thickness of 20 Å was obtained.

For a variety of applications where molecular recognition is needed, such as shape-selective catalysis, molecular sieving, and selective adsorption, mesostructured material with small pore size may lead to mass-transfer limitations or decreased accessibility to active sites [17–19]. For catalytic reactions, such as propane (amm)oxidation, the influence of internal diffusion could be gauged by the value of an effective diffusivity and Thiele Modulus [20]. The increase in pore size and pore volume leads to reduced mass transfer effects. Therefore, porous materials displaying tailored pore size and shape are particularly attractive for catalytic applications. However, there are no reports of mesoporous niobium oxides with tunable pore structures.

In this paper, we describe a new application of evaporation induced self-assembly (EISA) [7, 21] to obtain thermally stable and well-defined mesoporous niobium oxides with tunable pore structures. This method enabled us to obtain mesoporous Nb_2O_5 using nonionic surfactants and, more importantly, to tune their pore structure by adjusting the aging conditions. Moreover, surfactant mixtures containing nonionic amphiphilic triblock copolymer Pluronic P123 ($EO_{20}PO_{70}EO_{20}$) and Brij 35 ($C_{12}H_{25}EO_{23}$) were employed for the very first time in the synthesis in order to control the pore structure of resultant mesoporous Nb_2O_5. Mesoporous niobium oxides were obtained for the very first time exhibiting mesopore sizes in a wide range from 4.6 to 21 nm which were stable up to 500 °C after the removal of the surfactants.

Experimental

Chemicals

All chemicals were commercially available. Triblock copolymer surfactant ($HO(CH_2CH_2O)_{20}(CH_2CH(CH_3)O)_{70}(CH_2CH_2O)_{20}H$ designated as $EO_{20}PO_{70}EO_{20}$, Pluronic P123; Average molecular weight $M_{av} = 5800$, BASF), oligomeric alkyl-ethylene oxide surfactant (Brij 35, namely $C_{12}H_{25}EO_{23}$, average molecular weight $M_{av} = 1198$, Aldrich), anhydrous niobium chloride (99%, Alfa Aesar), and Ethanol (EtOH, for industrial use, AAPER Alcohol and Chemical Co.) were used as received.

Synthesis

Mesostructured niobium oxides were synthesized as follows. In a typical synthesis, 1 g of $EO_{20}PO_{70}EO_{20}$ was dissolved in 10–20 g of ethanol (EtOH). About 0.005–0.01 mol $NbCl_5$ precursor was added into the surfactant solution with vigorous stirring for 0.5 h. About 1–5 g of deionized water was added in the surfactant-Nb solution. The resulting sol solution was aged at 40 °C, 90 °C, 105 °C, and 115 °C for 2–6 days in the atmosphere with relative humidity (RH) of 20–70%. The as-synthesized samples were calcined at 400 °C, 500 °C, and 600 °C for 3–5 h in air to remove the surfactant. In the mixed surfactant cases, the total amount of P123 and Brij 35 was kept constant in all syntheses and the molar Brij 35 to P123 ratio was 0.5, 1.0, and 1.5.

Characterization

The small angle X-ray scattering (SAXS) patterns were collected using Rigaku RU-V 200 generator and Cu Kα radiation. The LabView module (National Instruments, Inc.) was used to collect the data. Wide-angle X-ray scattering (WAXS) patterns were obtained using Siemens D-500 diffractometer and Cu Kα radiation with a step rate of 0.02°/s. The N_2 adsorption–desorption isotherms were measured at 77 K using Micromeritics Tri-Star 3000 porosimeter. The pore size distributions and surface areas were determined by the Barrett–Joyner–Halenda (BJH) [22] and Brunauer–Emmett–Teller (BET) [23] methods, respectively. The pore volumes were calculated by the BJH method. Scanning transmission microscopy (STEM) studies were carried out on a Joel-2010 electron microscope operating at 200 kV with a GATAN CCD camera, using 2 Å probe with high angle dark field detector.

Results and discussion

The SAXS pattern of a representative mesoporous niobium oxide (sample A in Table 1) after calcination at 400 °C is shown in Fig. 1. One primary diffraction peak was present at $d = 70$ Å, which indicated a somewhat disordered pore structure. It was tentatively assigned to a 2D hexagonal structure with the unit cell parameter $a_0 = 81$ Å. The absence of high 2θ angle reflections in the XRD pattern of the calcined niobium oxide (not shown) indicated the

Table 1 Pore properties of mesostructured niobium oxide after calcination at different temperatures T_C

Sample	T_C (°C)	S_{BET} (m^2/g)	S_{theory}[a] (m^2/g)	V_P (cm^3/g)	D (nm)
A	400	211	221	0.26	4.7
A-5	500	165	196	0.22	4.5
A-6	600	41	33	0.18	22

S_{BET}, BET surface area; S_{theory}, Theoretical surface area; V_P, BJH pore volume; D, BJH pore size

[a] Assuming uniform and cylindrical pores, $S_{theory} = 4V_P/D$

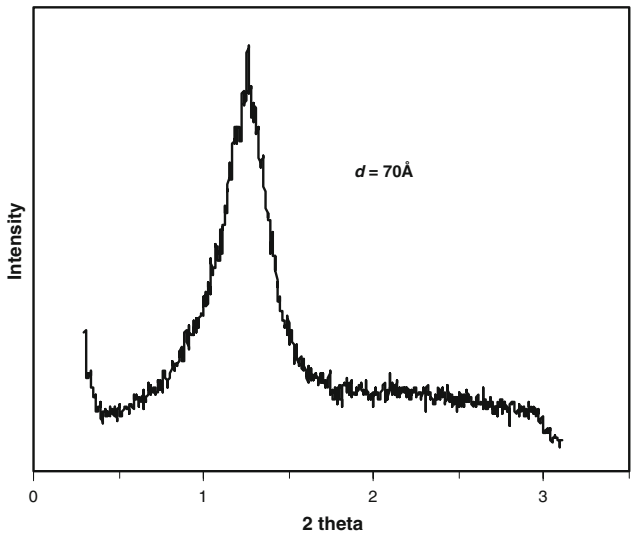

Fig. 1 SAXS pattern of mesoporous niobium oxide (sample A in Table 1) after calcination at 400 °C

amorphous nature of the inorganic walls in this mesoporous oxide. Scanning transmission electron microscopy (STEM) study was carried out on the same niobium oxide sample (sample A in Table 1) which indicated the presence of a ordered mesostructure with uniform ~5 nm diameter pore spacing and ~4 nm wall spacing (Fig. 2a, b). The N_2 adsorption–desorption isotherms of this mesoporous niobium oxide sample are shown in Fig. 3. A typical type-IV isotherm was observed. Large H1-type hysteresis loops were present in the isotherms of the mesoporous niobium oxide, which are characteristic of cylindrical pore geometry and a high degree of pore size uniformity [24, 25]. This mesoporous niobium oxide possessed the surface area of 211 m^2/g and pore volume of 0.26 cm^3/g. The BJH analysis indicated that this calcined mesoporous niobium oxide exhibited an average pore size of 47 Å (Fig. 3 inset) in agreement with STEM data (Fig. 4).

The thermal stability was investigated by varying the calcination temperature from 400 °C to 600 °C for the same mesoporous niobia sample. The absence of high 2θ angle reflections in the wide-angle X-ray scattering (WAXS) pattern of mesoporous niobia after calcination at

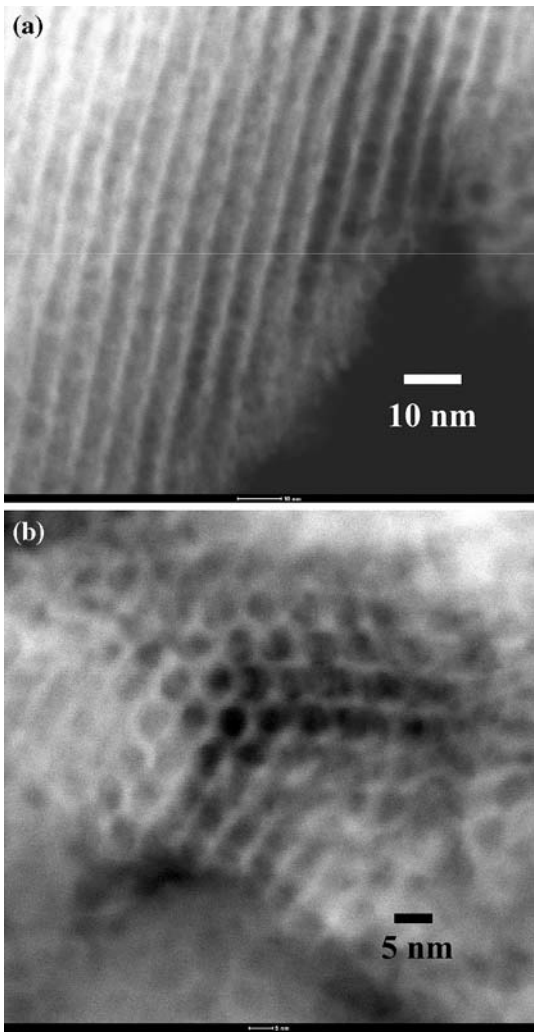

Fig. 2 Dark-field STEM Images of mesoporous niobium oxide (sample A in Table 1) after calcination at 400 °C: a uniform appearance of channels and hexagonal arrays of mesopores

400 °C and 500 °C (samples A and A-5 in Table 1) indicated the amorphous nature of the inorganic walls in these mesoporous oxides. A diffraction peak in the SAXS pattern of the sample A-5 (not shown) was present at the d-spacing of 67 Å indicating further condensation in the inorganic walls after calcination at a higher temperature which led to the unit cell contraction. The mesostructure of sample A-5 was preserved after calcination at 500 °C, but its surface area decreased to 165 m^2/g, while the pore volume and pore size became 0.22 cm^3/g and 4.5 nm, respectively. After calcination at 600 °C, four intense diffraction peaks were observed, which can be indexed as (001), (100), (101), (002) reflections of crystalline niobium oxide (JCPDS#07-0061) [26]. The crystalline domain size based on the (100) reflection was 13 nm estimated according to Scherrer's formula [$t = K\lambda/(B \cos \theta)$]. The surface area of this niobium oxide decreased to 41 m^2/g, whereas the pore

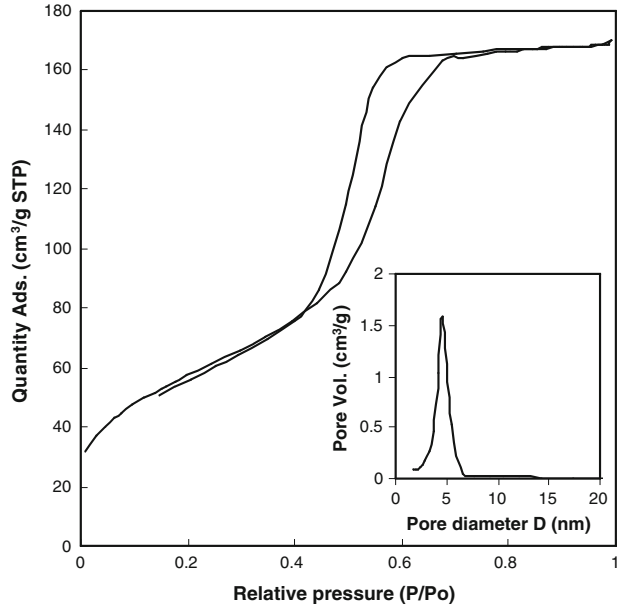

Fig. 3 N_2 adsorption–desorption isotherms of mesoporous niobium oxide (sample A in Table 1) calcined at 400 °C and BJH pore size distribution plot (inset) of its adsorption branch

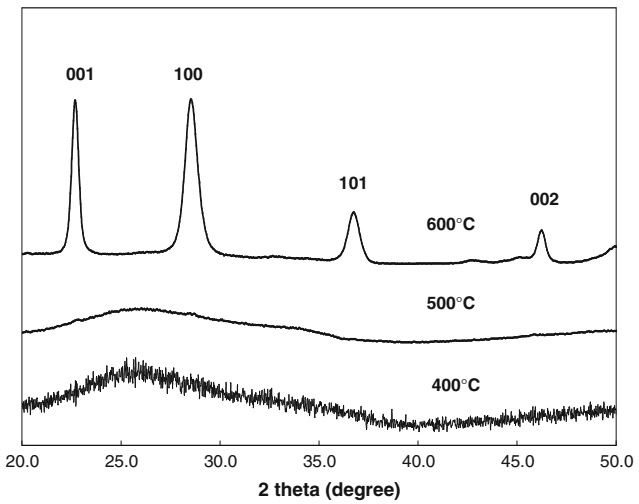

Fig. 4 Wide-angle X-ray diffraction patterns of calcined mesoporous niobium oxide at 400 °C, 500 °C, and 600 °C (sample A, A-5, and A-6 in Table 1)

size increased to 22 nm. It was noted that as the calcination temperature increased above 500 °C, the amorphous niobium oxide crystallized and nanocrystallite size increased rapidly. For those samples which exhibited significant pore size increase upon calcination and contained nanocrystals larger than the mesostructure wall thickness, the surface areas and pore volumes corresponded to interparticle porosity of the aggregated niobium oxide nanocrystals.

The nitrogen adsorption–desorption isotherms and pore size distributions of mesoporous niobium oxides (sample A, B, C, and D in Table 2) obtained at different aging temperatures (40 °C, 90 °C, 105 °C, and 115 °C) followed by calcination at 400 °C are shown in Fig. 5. The BJH pore size analysis performed on the adsorption branches showed that these four samples exhibited a mean pore size of 4.7, 9, 14, and 21 nm, respectively, when the aging temperature increased. The positions of the hysteresis loops of samples A to D shifted to higher pressures as the aging temperature increased, indicating the increase of pore size with increasing aging temperature. The increase in pore size with aging temperatures can be explained by the temperature-dependent behavior of the $(EO)_x(PO)_y(EO)_x$ triblock copolymers in acidic media [27–29]. As the hydrophobicity of the EO blocks increases with the temperature, the EO chains withdraw inside the hydrophobic (PO) core of the surfactant, resulting in a larger volume of the micelle core and, therefore, a larger average pore diameter and higher pore volume of the material [29]. During calcinations, some micropores resulted from the EO chain withdraw may merge to form larger pores. The BJH pore volumes and BET surface areas are shown in Table 2 together with theoretical estimates of the surface areas. Theoretical surface areas (S_{theory}) were estimated as $S_{theory} = 4V_P/D$, which assumes the presence of uniform cylindrical pores with the BJH pore volume V and pore diameter D. The experimental BET surface areas were higher than the theoretical estimates suggesting the presence of structural microporosity, which is consistent with earlier observations of structurally similar mesoporous SBA-15 silicas [30]. In the case of SBA-15 silica, the EO chains of the template partially penetrated the inorganic walls and created microporosity within the inorganic walls after surfactant removal [30]. To the best of our knowledge, it is the first time that mesoporous niobium oxides were obtained possessing the pore size larger than those reported previously

Table 2 Pore properties of mesoporous niobium oxide prepared at different aging conditions (aging at RH = 20% for 2 days except for sample E and F; calcination at 400 °C)

Sample	Aging temperature (°C)	S_{BET} (m^2/g)	S_{theory} [b] (m^2/g)	V_P (cm^3/g)	D (nm)
A	40	211	221	0.26	4.7
B	90	201	187	0.42	9
C	110	189	140	0.49	14
D	115	184	101	0.53	21
B	110 (2 days)	189	140	0.49	14
E	110 (6 days)	176	122	0.61	20
A	40	211	221	0.26	4.7
F	40-H[a] (2 days)	202	211	0.39	7.4

S_{BET}, BET surface area; S_{theory}, Theoretical surface area; V_P, BJH pore volume; D, BJH pore size

[a] H-RH = 70%

[b] Assuming uniform and cylindrical pores, $S_{theory} = 4V_P/D$

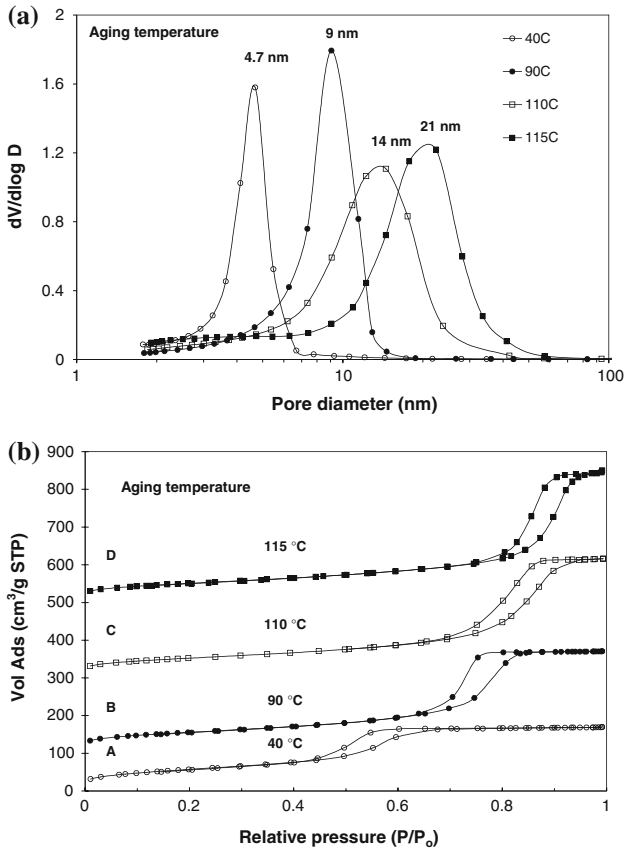

Fig. 5 (**a**) BJH pore size distribution plots based on N_2 adsorption branches for mesostructured niobium oxide (samples A, B, C, and D in Table 2) aged at 40 °C, 90 °C, 110 °C, and 115 °C followed by calcination at 400 °C. (**b**) N_2 adsorption–desorption isotherms of mesostructured niobium oxide (samples A, B, C, and D in Table 2) aged at 40 °C, 90 °C, 110 °C, and 115 °C followed by calcination at 400 °C (vertical offset was applied)

(∼5 nm) [14] when only Pluronic P123 surfactant was employed as the structure-directing agent without the addition of pore swelling agents.

Lower surface areas, larger pore volumes and pore sizes were observed in the resultant mesoporous niobium oxides when the aging time increased from 2 to 6 days (corresponding to sample C and E in Table 2). The N_2 adsorption–desorption isotherms for these two samples exhibited significant differences (Fig. 6). Sample E aged for 6 days exhibited a more regular H1-type hysteresis loop than that observed in sample C which was aged for 2 days indicative of a slight mesopore structural change [31] in this niobia sample obtained after longer aging time. Further condensation and cross-linking in the niobium oxide framework with increasing aging time enhanced the strength and stiffness of the as-synthesized niobium oxide and increased the mesoporosity, which resulted in larger pore size. Longer aging time also facilitated generation of micropores which increased the total pore volume [32]. Some micropores may merge into larger pores.

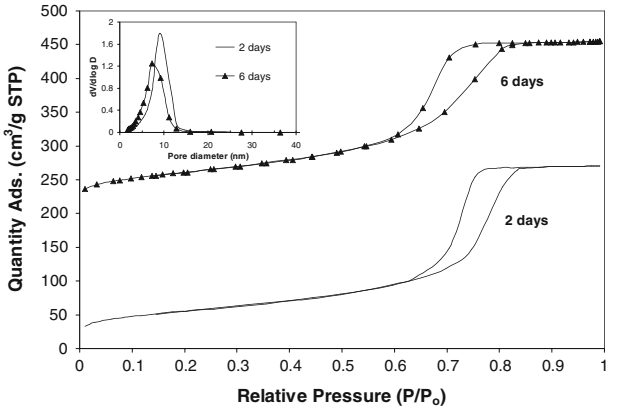

Fig. 6 N_2 adsorption–desorption isotherms of mesostructured niobium oxide (samples C and E in Table 2) aged at 110 °C for 2 and 6 days followed by calcination at 400 °C (Inset: BJH pore size distribution plots based on N_2 adsorption branches. Vertical offset was applied)

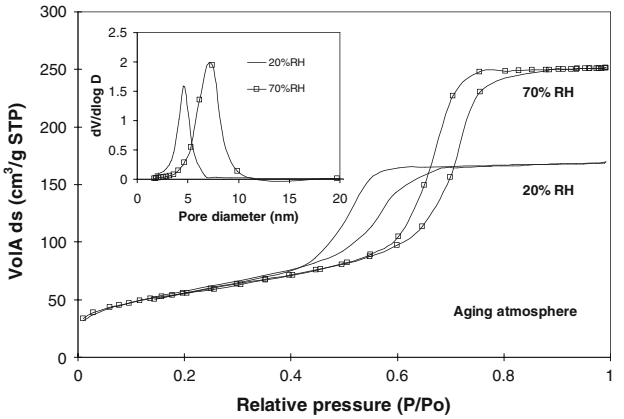

Fig. 7 N_2 adsorption–desorption isotherms of mesostructured niobium oxide (samples A and F in Table 2) aged at different humidity conditions and followed by calcination at 400 °C (Inset: BJH pore size distribution plots based on N_2 adsorption)

It was demonstrated that the humidity of aging atmosphere during the EISA process had a significant influence on the mesostructural order, for example, by increasing the flexibility of structural reorganization [33]. The impact of relative humidity during aging on the mesopore structure was investigated and the representative results are shown in Table 2 and Fig. 7. Samples A and F were aged in air at different relative humidity (RH). The sample F possessed larger pore size after aging at 70% RH than sample A obtained at 20% RH. The comparison of their N_2 adsorption–desorption isotherms suggested that more uniform cylindrical mesopores were obtained after aging at higher RH manifested in more regular and parallel N_2 adsorption and desorption branches. It indicated that surfactant segregation was also governed by the relative humidity, which controls the water evaporation from the sol solution [33].

Higher humidity during aging retains water in the as-synthesized material, slows down the water evaporation rate, dilutes the local concentration, and provides the necessary fluidity for the organization of template or even disorder-to-order transition [34].

Mesoporous structures may be controlled not only by varying the nature of inorganic species, surfactant concentration, reaction temperature, and humidity, but also by changing the effective hydrophilic–hydrophobic volume balance in the context of the classical micellar packing parameter [24, 35]. A mixture of two surfactants with different headgroup sizes may provide an effective means to change the hydrophilic–hydrophobic volume balance as demonstrated by Zhao et al. [31]. They showed that a less-ordered 2D hexagonal mesostructure of the silica materials obtained using pure Pluronic P123 can be changed to highly ordered 2D hexagonal structure when employing the blends of Brij 35 and Pluronic P123 surfactants. The degree of mesostructural order of the final silica products was improved significantly. However, there are no reports of using surfactant mixtures to improve mesostructural order in transition metal oxides and, in particular, in niobium oxide. Here, we explored the possibility of pore structure control of mesoporous niobium oxide.

Mesoporous niobium oxides were synthesized using the mixtures of amphiphilic triblock co-polymer Pluronic P123 and nonionic surfactants Brij 35. The pore properties of resultant mesoporous niobium oxide phases are listed in Table 3. As compared with mesoporous niobium oxide (sample B) templated by pure Pluronic P123 (denoted as P), the samples a and b prepared from the surfactant blends showed similar mesopore sizes. However, different mesopore shape was observed in sample b indicated by its N_2 sorption isotherms (Fig. 8). When the amount of Brij 35 (denoted as B) was increased in the mixture with the P123-to-Brij 35 (P/B) ratio of 0.5 (Table 3), the mesopore size decreased to 7.8 nm and the sorption hysteresis loop transformed from the H1 to H2 type. The EO/PO ratio

Table 3 Pore properties of mesoporous niobium oxide synthesized employing surfactant mixtures of Pluronic P123 and Brji 35 in their molar ratio of P/B

Sample	P:B (mol)	EO/PO (mol)	S_{BET} (m^2/g)	S_{theory} (m^2/g)	V_P (cm^3/g)	D (nm)
B	P:0	40/70	201	187	0.42	9
a	1.5	33/42	205	177	0.42	9.5
b	1.0	32/35	188	156	0.39	10
c	0.5	29/23	159	144	0.28	7.8
d	0:B	23/–	174	165	0.19	4.6

Aging temperature, 90 °C; Calcination temperature, 400 °C. S_{BET}, BET surface area; S_{theory}, theoretical surface area; V_P, BJH pore volume; D, BJH pore size

* Assuming uniform and cylindrical pores, $S_{theory} = 4V_P/D$

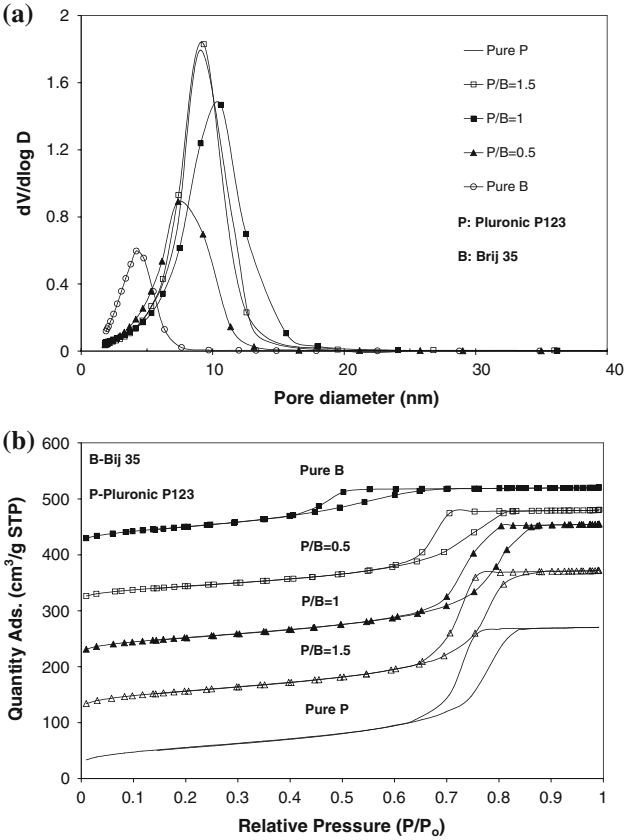

Fig. 8 (**a**) BJH pore size distribution plots based on N_2 adsorption branches for mesostructured niobium oxide (samples B, a, c, and d in Table 3) synthesized employing surfactant mixtures (Pluronic P123 and Brij 35). (**b**) N2 adsorption–desorption isotherms of mesostructured niobium oxide (samples B, a, b, c, and d in Table 3) synthesized employing surfactant mixtures (Pluronic P123 and Brij 35) (vertical offset was applied)

shown in Table 3 indicated dramatic volume reduction in hydrophobic cores of PO chains, replaced by shorter alkyl chains of Brij 35 as the synthesis P123/Brij 35 ratio was increased thus explaining the decrease in the surface area, pore volume, and pore size of resultant mesoporous phases. Mesoporous niobia obtained in the presence of Brij 35 only exhibited a pore size of 4.6 nm. Based on these results, the ordering of mesostructural niobium oxides did not significantly improve when surfactant mixtures were employed. However, it suggested that the mesopore structure can be changed from cylindrical to ink-bottle pore structure (the hysteresis loop shifted from the H1 to H2 type) in the presence of shorter molecular chains of Brij 35.

The comparison of pore properties of mesoporous niobium oxide prepared in this study and reported in literature is shown in Table 4. It is clear that the mesoporous niobium oxide phases obtained in this study possessed highly attractive features, namely high surface areas, large pore volumes, and tunable pore sizes in a wide range of 4.6–21 nm.

Table 4 Comparison of pore properties of mesoporous Nb_2O_5 phase obtained in this and previous studies

Niobium oxide	S_{BET} (m^2/g)	V_P (cm^3/g)	D (nm)	Reference
1	434	–	2.7	[8]
2	196	0.22	5	[11]
3	118–173	0.14–0.29	3.8–4.9	[13]
4	144–211	0.19–0.61	4.7–21	This study

Conclusions

We reported a new successful application of EISA process for preparing thermally stable and well-defined 2D mesostructured niobia phases. The pore size of mesoporous niobium oxides was for the first time tuned in a wide range from 4.6 to 21 nm by varying aging temperature, aging time, and the humidity of aging atmosphere. Mixtures of two nonionic surfactants, Pluronic P123 and Brij 35, were for the first time used to tune the pore structure of resultant mesoporous niobium oxide phases which showed that the shape of mesopores in niobium oxide may be changed from cylindrical to ink-bottle. The mesostructures of niobium oxides prepared in this study were thermally stable up to 500 °C. These novel mesoporous niobium oxides with tunable pore sizes are highly attractive as catalytic supports or a major component in the synthesis of complex mixed metal oxide catalysts for selective oxidation of lower alkanes.

Acknowledgements This research was supported by the National Science Foundation under NSF CAREER Award CTS#0238962 to Dr. Vadim V. Guliants.

References

1. (a) Tanabe K (1990) Catal Today 8:1. doi:10.1016/0920-5861(90)87003-L; (b) Japan Patent Kokai (1987) 62-27 043, to Nippon Shokubai Co. Ltd; (c) US Patent 4,665,200 (1987), to Nippon Shokubai Co. Ltd; (d) US Patent 4,781,862 (1988), to Montvale Process Co. Inc.
2. Desponds O, Keiski RL, Somorjai GA (1993) Catal Lett 19:17
3. Jehng JM, Turek AM, Wachs IE (1992) Appl Catal 83:179. doi:10.1016/0926-860X(92)85034-9
4. Deo G, Wachs IE (1991) J Catal 129:307. doi:10.1016/0021-9517(91)90036-4
5. Wachs IE, Jehng JM, Deo G, Hu H, Arora N (1996) Catal Today 28:199. doi:10.1016/0920-5861(95)00229-4
6. Smits RHH, Seshan K, Leemreize H, Ross JRH (1993) Catal Today 16:513
7. Yuan L, Bhatt S, Beaucage G, Guliants VV, Mamedov S, Soman RS (2005) J Phys Chem B 109:23250. doi:10.1021/jp054218p
8. Evans OR, Bell AT, Tilley TD (2004) J Catal 226:292. doi:10.1016/j.jcat.2004.06.002
9. Sun G, Xu A, He Y, Yang M, Du H, Sun C (2008) J Hazard Mater 156:335. doi:10.1016/j.jhazmat.2007.12.023
10. Antonelli DM, Ying JY (1996) Angew Chem 108:461. doi:10.1002/ange.19961080413
11. Antonelli DM, Ying JY (1996) Angew Chem Int Ed Engl 35:426. doi:10.1002/anie.199604261
12. Antonelli DM, Nakahira A, Ying JY (1996) Inorg Chem 35:3126. doi:10.1021/ic951533p
13. Sun T, Ying JY (1998) Angew Chem Int Ed 37:664. doi:10.1002/(SICI)1521-3773(19980316)37:5<664::AID-ANIE664>3.0.CO;2-T
14. Yang PD, Zhao DY, Margolese DI, Chmelka BF, Stucky GD (1999) Chem Mater 11:2813. doi:10.1021/cm990185c
15. Lee B, Lu DL, Kondo JN, Domen K (2002) J Am Chem Soc 124:11256. doi:10.1021/ja026838z
16. Katou T, Lu DL, Kondo JN, Domen K (2002) J Mater Chem 12:1480. doi:10.1039/b200380e
17. Altwasser S, Glaser R, Weitkamp J (2007) Microporous Mesoporous Mater 104:281. doi:10.1016/j.micromeso.2007.02.046
18. Song C, Garcés JM, Sugi Y (2000) Shape-selective catalysis: chemicals synthesis and hydrocarbon processing. ACS symposium series 738, Oxford University Press
19. Thomas JM, Raja R (2007) Top Catal 40:3. doi:10.1007/s11244-006-0105-7
20. Levenspiel O (1999) Chemical reaction engineering, 3rd edn. Wiley, New York
21. Brinker CJ, Lu Y, Sellinger A, Fan H (1999) Adv Mater 11:579. doi:10.1002/(SICI)1521-4095(199905)11:7<579::AID-ADMA579>3.0.CO;2-R
22. Barrett EP, Joyner LG, Halenda PP (1951) J Am Chem Soc 73:373. doi:10.1021/ja01145a126
23. Brunauer S, Emmett PH, Teller E (1938) J Am Chem Soc 60:309. doi:10.1021/ja01269a023
24. Huo Q, Margolese D, Stucky GD (1996) Chem Mater 8:1147
25. Kruk M, Jaroniec M, Sayari A (1997) Langmuir 13:6267. doi:10.1021/la970776m
26. Frevel R (1955) Anal Chem 27:1329. doi:10.1021/ac60104a035
27. Zhao DY, Feng JL, Huo QS, Melosh N, Fredrickson GH, Chmelka BF et al (1998) Science 279:548. doi:10.1126/science.279.5350.548
28. Galarneau A (2001) Langmuir 17:8328. doi:10.1021/la0105477
29. Voort P, Benjelloun M, Vansant E (2002) J Phys Chem B 106:9027. doi:10.1021/jp0261152
30. Goltner-Spickermann C (2002) Curr Opin Colloid Interface Sci 7:173. doi:10.1016/S1359-0294(02)00046-8
31. Tian B, Liu X, Zhang Z, Tu B, Zhao DY (2002) J Solid State Chem 167:324
32. Smitha S, Shajesh P, Aravind PR, Kumar SR, Pillai PK, Warrier KGK (2006) Microporous Mesoporous Mater 91:286. doi:10.1016/j.micromeso.2005.11.051
33. Crepaldi E, Soler-Illia GJAA, Bouchara A, Grosso D, Durand D, Sanchez C (2003) Angew Chem Int Ed 42:347. doi:10.1002/anie.200390113
34. Crepaldi E, Soler-Illia GJAA, Grosso D, Cagnol F, Ribot F, Sanchez C (2003) J Am Chem Soc 125:9770. doi:10.1021/ja030070g
35. Huo Q, Leon R, Petroff PM, Stucky GD (1995) Science 268:1324. doi:10.1126/science.268.5215.1324